Current-biased Andreev interferometer

Artem V. Galaktionov[1,2] and Andrei D. Zaikin[1,2,3]

[1]*I.E. Tamm Department of Theoretical Physics, P.N. Lebedev Physical Institute, 119991 Moscow, Russia*
[2]*Laboratory of Cryogenic Nanoelectronics, Nizhny Novgorod State Technical University, 603950 Nizhny Novgorod, Russia*
[3]*Institute of Nanotechnology, Karlsruhe Institute of Technology (KIT), 76021 Karlsruhe, Germany*

We theoretically investigate the behavior of Andreev interferometers with three superconducting electrodes in the current-biased regime. Our analysis allows us to predict a number of interesting features of such devices, such as both hysteretic and nonhysteretic behavior, negative magnetoresistance, and two different sets of singularities of the differential resistance at subgap voltages. In the nonhysteretic regime we find a pronounced voltage modulation with the magnetic flux which can be used for improving the sensitivity of Andreev interferometers.

I. INTRODUCTION

It was demonstrated experimentally by Petrashov and co-workers,[1] as well as by several other experimental groups,[2] that the resistance of mesoscopic diffusive normal-superconducting (NS) hybrid structures can be quite strongly modulated by an externally applied magnetic field. These observations open a possibility to construct the so-called Andreev interferometers which, for a number of applications, may have several important advantages over the well-known superconducting quantum interference devices (SQUIDs). Such types of applications may include, e.g., the possibility to implement the readout of superconducting qubits[3] or the experimental analysis of the switching dynamics of individual magnetic nanoparticles[4] that require features of a detector such as reduced intrinsic dissipation (down to the fW level), the possibility to achieve higher sensitivity and readout speed, as well as a broad choice of normal conductors employed as a weak link.

Recently, there were both experimental[5] and theoretical[6,7] investigations of hybrid NS structures with pronounced dependencies of their resistance on the applied magnetic flux (see also earlier theoretical works[8,9] where other realizations were analyzed). Contrary to the initial design of Andreev interferometers pioneered by Petrashov and coauthors,[1] this latest analysis focuses on the systems with all external electrodes in the superconducting state. In this way one would be able to reduce dissipation. Current (voltage) harmonics would be generated in this case, which are multiples of the Josephson frequency. However, they can be filtered out and the average current (voltage) can be measured, which should reveal a dependence on the magnetic flux.

It is worth pointing out that the study of structures with several superconducting electrodes attached to a piece of a normal metal has a history of its own. For example, the "Josephson triode" was dealt with in Ref. 10 by means of Aslamazov-Larkin theory combined with the resistively shunted junction (RSJ) model. A similar approach was employed[11] in order to analyze the behavior of multiterminal Josephson junctions. Interesting features of such structures, such as, e.g., bistable states and magnetic flux transfer, were demonstrated theoretically in the ballistic limit.[12] One can also mention a modification of Shapiro steps in multiterminal structures.[13]

In Ref. 7 we already carried out a detailed theoretical analysis of Andreev interferometers in the voltage-biased regime. While this regime can be realized in some experiments, of clear experimental interest is also another physical situation when the system is biased by a fixed external current. The main purpose of the present work is to analyze the behavior of Andreev interferometers in the current-biased regime.

Note that the system behavior in the latter regime can be very different from that in the voltage-biased one. In a vast majority of normal structures these differences mainly concern higher cumulants of voltage and current. For instance, a decade ago there arose a conundrum caused by experiments,[14] where the third voltage cumulant of the current-biased normal junction was measured. The behavior of this quantity was essentially different from theoretical expectations based on the linear relation between the third voltage correlator in the current-biased regime and the third current correlator[15–17] in the voltage-biased regime. This conundrum was resolved in Ref. 18, where the major conclusion was that current and voltage correlators of order three and higher are no longer linearly related.

In superconducting circuits essential differences between the voltage- and current-biased regimes occur already at the level of I-V curves. Such differences were encountered, e.g., in the case of single Josephson junctions[19] (see also Ref. 20). A profound qualitative distinction between these regimes is caused by the fact that, as it was demonstrated in Ref. 19, in the current-biased limit the Cooper pair current may provide a major contribution to the dissipative current flowing in the device. Technically, this contribution is related to the kernel $S_2(t)$ in the current-phase relationship [see Eqs. (5) and (6) below] originating from anomalous Green's functions. In contrast, in the voltage-biased regime the dissipative contribution to the current is mainly due to quasiparticles [accounted for by the kernel $S_1(t)$—see below] in combination with multiple Andreev reflections (provided the system transparency is not too small). This qualitative difference between the regimes results in entirely different current-voltage characteristics in the subgap region. Earlier experiments[21] conformed to the predictions.[19] Later, further experimental support to this theoretical picture was obtained[22–24] (see also the corresponding discussion in Chap. 4 of Ref. 20). Another example is the low temperature

behavior of Josephson junction arrays and chains which may vary from superconducting to insulating depending on whether the voltage- or current-biased scheme is considered.[25]

The structure of our paper is as follows. In Sec. II we describe the model for Andreev interferometers under consideration. In Sec. III we proceed with a theoretical analysis of our model and derive the basic formula that fixes the current-phase relation for our device. This formula is then employed in Sec. IV, where we numerically evaluate the I-V curve for our system in the current-biased regime and study the effect of voltage modulation by an external magnetic flux. The paper is concluded by a brief discussion of our key observations in Sec. V. Some technical details are relegated to the Appendix.

II. THE MODEL

The system under consideration is schematically depicted in Fig. 1. It consists of three superconducting electrodes characterized by the absolute value of the order parameter Δ and a disordered normal metal insertion embedded between these electrodes. A typical size L of this normal metallic dot is assumed not to exceed the superconducting coherence length ξ and at the same time to be larger than the elastic mean free path ℓ. Two superconducting electrodes 2 and 3 form a loop which is pierced by an external magnetic flux Φ. Accordingly, the superconducting phase difference $\chi = 2\pi\Phi/\Phi_0$ is induced between electrodes 2 and 3, where Φ_0 is the superconducting flux quantum.

In what follows we will generally assume that all interfaces between the normal metal and superconducting electrodes are weakly transmitting. In this case one can expect to observe a pronounced magnetoresistance modulation effect.[26] For comparison, in the limit of highly transparent NS interfaces, this modulation is expected to remain below 10%.[26,27] The
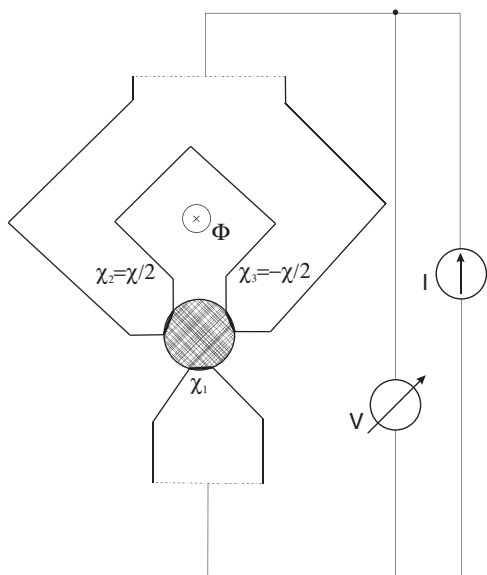

FIG. 1. Scheme of the setup: Disordered normal metal insertion (dot) embedded between three superconducting electrodes. The phase difference $\chi_2 - \chi_3 = \chi$ is caused by the magnetic flux Φ piercing the loop.

normal state conductances G_1, G_2, and G_3 between three electrodes and the normal insertion obey the condition

$$G_1 \equiv \frac{1}{R_N} \ll G_{2,3} \ll \sigma_D \mathcal{A}/L, \qquad (1)$$

where the normal state resistance R_N is determined by the standard Landauer formula

$$\frac{1}{R_N} = \frac{e^2}{\pi} \sum_n T_n, \qquad (2)$$

T_n are the transmissions of conducting channels in the first barrier, $\sigma_D = 2e^2 D N_0$ is the Drude conductivity of the normal metal, $\mathcal{A}$ denotes a typical contact area between the normal metal and the electrode, $D = v_F \ell/3$ is the diffusion coefficient, and N_0 is the density of states at the Fermi surface per spin direction. The electron charge will be denoted by $-e$.

Equation (1) assures that the voltage drop occurs only across the tunnel barrier between the first electrode and the rest of our system. The second inequality (1) also guarantees that our results will not depend on the particular shape of the normal metal insertion. In addition, we will disregard charging effects, which amounts to assuming that all relevant effective charging energies remain much smaller than other important energy scales in our problem.[28]

As we already discussed, below we will be interested in the current-biased regime, i.e., we will assume that our system is biased by an external current source I, as is indicated in Fig. 1. Restricting ourselves to this regime we will evaluate the time-averaged voltage V across our device, which should depend both on the bias current I and on the external flux Φ (or, equivalently, on the phase difference χ). In the case of Josephson junctions with normal state resistance R_N and capacitance C it was demonstrated[19] that the I-V curves in the current- and voltage-biased regimes differ substantially provided the parameter $\beta = \Delta R_N C$ remains smaller than one. Below we will also stick to the same limit, $\beta \ll 1$.

III. CURRENT-PHASE RELATIONS

The first step to derive the current-voltage characteristics is to establish the dependence of the instantaneous current value $I(t)$ on the phase difference $\varphi(t)$ across the NS interface with the smallest conductance $1/R_N$. This phase difference is defined by the standard relation

$$\varphi(t) = e \int_0^t dt' V(t'), \qquad (3)$$

where $V(t)$ is the time-dependent voltage drop across this NS interface. In order to accomplish this goal one can employ the effective action analysis.[28–30] The general Keldysh effective action describing electron transport across the barrier between the first superconducting electrode and the rest of our structure has the form

$$\mathcal{S} = -\frac{i}{2} \sum_n \mathrm{Tr}\ln\left[1 + \frac{T_n}{4}\left(\{\check{g}_N, \check{g}_S\} - 2\right)\right]. \qquad (4)$$

Here $\check{g}_S$ is the Green-Keldysh matrix of the superconducting reservoir 1 and $\check{g}_N$ is the 4×4 Green-Keldysh matrix of a disordered normal metal which also acquires superconducting properties due to the contact with reservoirs 2 and 3.

The effective action (4) holds for arbitrary transmission values T_n and allows for a complete description of electron transport through our device. It is convenient to combine the phase variables on the two branches of the Keldysh contour and define the "classical" [$\varphi(t)$] and "quantum" [$\varphi_-(t)$] components of the phase. Taking the derivatives of the effective action with respect to the quantum phase φ_-, one can derive the expressions for all current correlators in our problem. Provided the charging effects are weak, the action (4) can be expanded in powers of φ_- and reduced to a much simpler form that is convenient for practical calculations. In the case of NS hybrid structures this procedure was described in detail in Ref. 31.

Since here we are merely interested in the tunneling limit $T_n \ll 1$, it suffices to expand the action (4) up to the first order in T_n. Then taking the first variation of the action with respect to φ_-, one arrives at the current-phase relation in the form

$$I(t) = \int_0^t dt' \sin[\varphi(t) - \varphi(t')]S_1(t - t')$$
$$+ \int_0^t dt' \sin[\varphi(t) + \varphi(t')]S_2(t - t'). \quad (5)$$

To avoid possible confusion, let us mention that the voltage-related phase (3) is two times smaller than the superconducting phase difference across the tunnel junction.

As is usual in the tunneling limit, the kernels $S_1(t)$ and $S_2(t)$ are expressed respectively via normal and anomalous components of the Green-Keldysh matrices, calculated for an infinitely high tunnel barrier between the normal insertion and the first electrode, i.e.,

$$S_1(t) = -\frac{ie}{4}\sum_n T_n \left[g_S^R(t)g_N^K(-t) + g_S^K(t)g_N^A(-t) \right.$$
$$\left. + g_N^R(t)g_S^K(-t) + g_N^K(t)g_S^A(-t) \right],$$
$$S_2(t) = \frac{ie}{4}\sum_n T_n \left[f_S^R(t)f_N^K(-t) + f_S^K(t)f_N^A(-t) \right.$$
$$\left. + f_N^R(t)f_S^K(-t) + f_N^K(t)f_S^A(-t) \right]. \quad (6)$$

Note that Eqs. (5) and (6) can also be derived by means of the standard tunneling Hamiltonian approach.

What remains is to define the Green's functions of both the superconducting electrode and the normal metal dot. Without any loss of generality one can set the electric potential of the first superconducting electrode equal to zero. Then the Fourier transforms of $g_S^{R,A}$ and $f_S^{R,A}$ take the form

$$g_S^{R,A}(\epsilon) = \frac{\epsilon}{\xi^{R,A}}, \quad f_S^{R,A}(\epsilon) = \frac{\Delta}{\xi^{R,A}}. \quad (7)$$

In order to properly account for the analytic properties of the functions $\xi^{R,A}$ it is important to keep an infinitesimally small imaginary part $i0$, i.e.,

$$\xi^{R,A} = \pm\sqrt{(\epsilon \pm i0)^2 - \Delta^2}. \quad (8)$$

As the cut in the complex plane goes from $-\Delta$ to Δ, we obtain $\xi^{R,A} = \pm\text{sgn}\,\epsilon\sqrt{\epsilon^2 - \Delta^2}$ for $|\epsilon| > \Delta$ and $\xi^{R,A} = i\sqrt{\Delta^2 - \epsilon^2}$ for $|\epsilon| < \Delta$.

The Keldysh components g^K and f^K are related to the above retarded and advanced Green's functions in the standard manner as

$$g^K(\epsilon) = [g^R(\epsilon) - g^A(\epsilon)]\tanh\frac{\epsilon}{2T},$$
$$f^K(\epsilon) = [f^R(\epsilon) - f^A(\epsilon)]\tanh\frac{\epsilon}{2T}. \quad (9)$$

Now let us turn to the Green-Keldysh functions of the metallic dot $g_N^{R,A,K}$ and $f_N^{R,A,K}$. These functions have already been evaluated elsewhere,[7,9] therefore here we only briefly recapitulate the corresponding results. It is important to bear in mind that, due to the contact with superconducting terminals 2 and 3, the normal metal also acquires superconducting properties. For instance, the proximity-induced minigap Δ_g in its spectrum develops. This minigap is defined by the equation[7]

$$\Delta_g = \frac{\epsilon_g}{1 + \gamma\sqrt{1 - \Delta_g^2/\Delta^2}}, \quad (10)$$

where the quantity

$$\epsilon_g = \Delta\sqrt{1 - \frac{4G_2 G_3}{(G_2 + G_3)^2}\sin^2\frac{\chi}{2}} \quad (11)$$

depends on the external magnetic flux Φ via the phase difference χ. The parameter γ (Ref. 9) effectively controls the strength of electron-hole dephasing in our system. This parameter is defined as

$$\gamma = \frac{2\sigma_D \mathcal{V}\Delta}{D(G_2 + G_3)}, \quad (12)$$

where $\mathcal{V}$ stands for the volume of the normal metal.

In order to correctly determine the analytic properties of the Green's functions, we observe that the structure of the cuts in the complex plane is somewhat more complicated. Namely, these cuts are now located at $(-\infty, -\Delta]$, $[-\Delta_g, \Delta_g]$, and $[\Delta, \infty)$. As above, the retarded Green's functions are defined on the upper banks of these cuts. Provided $\Delta_g < \epsilon < \Delta$ we find

$$g_N^R(\epsilon) = \frac{\epsilon}{\sqrt{\epsilon^2 - \frac{\epsilon_g^2}{\left(1 + \gamma\sqrt{1 - \epsilon^2/\Delta^2}\right)^2}}},$$
$$f_N^R(\epsilon) = \frac{\epsilon_g}{\sqrt{\epsilon^2\left(1 + \gamma\sqrt{1 - \epsilon^2/\Delta^2}\right)^2 - \epsilon_g^2}}. \quad (13)$$

For the remaining values of ϵ the retarded Green's functions are obtained by analytic continuation with the mentioned cuts, while advanced Green's functions are defined as $g_N^A(\epsilon) = -[g_N^R(\epsilon)]^*$ and $f_N^A(\epsilon) = -[f_N^R(\epsilon)]^*$. Finally, the Keldysh components are again given by Eqs. (9).

Combining the above expressions for the Green's functions with Eqs. (6) it is easy to verify that $S_{1,2}(t < 0) \equiv 0$, i.e., both kernels (6) obey the requirement of causality. In the case of a Josephson junction between two BCS superconductors with different values of the gap, the kernels $S_{1,2}(\omega)$ were derived by Werthamer[32] and also by Larkin and Ovchinnikov.[33] For reference purposes the corresponding expressions [denoted below as $\tilde{S}_{1,2}(\omega)$] are presented in the Appendix. In our case the kernels $S_{1,2}(\omega)$ deviate from $\tilde{S}_{1,2}(\omega)$ since the energy spectrum of the central metallic dot is different from that of a
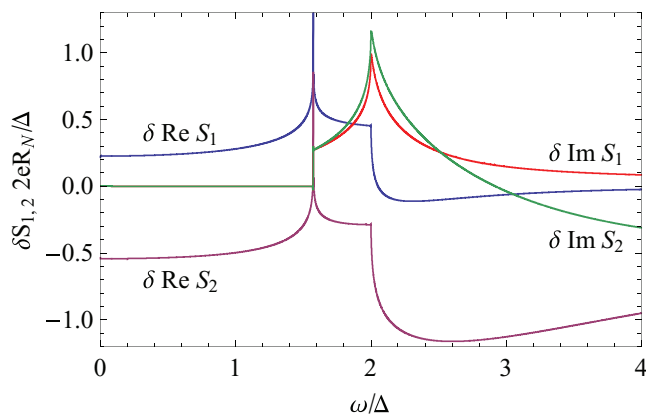
FIG. 2. (Color online) The functions $\delta S_{1,2}(\omega)$ (14) evaluated at $T \to 0$ for $\epsilon_g/\Delta = 0.95$ and $\gamma = 0.8$.

superconductor. The difference

$$\delta S_{1,2}(\omega) = S_{1,2}(\omega) - \tilde{S}_{1,2}(\Delta, \Delta_g, \omega) \qquad (14)$$

can be evaluated both numerically[34] and analytically in some limits. For illustration, in Fig. 2 we display the functions $\delta S_{1,2}(\omega)$ calculated at $\epsilon_g = 0.95\Delta$, $\gamma = 0.8$, and $T \to 0$.

Within the logarithmic accuracy an asymptotic behavior of $\mathrm{Re}\,\delta S_{1,2}(\omega)$ at $\omega \approx \Delta + \Delta_g$ is described as

$$\mathrm{Re}\,\delta S_{1,2}(\omega) \approx \frac{\Delta}{2eR_N}\sqrt{\frac{\Delta_g}{\Delta}}\left(\frac{1}{\sqrt{c_1}} - 1\right)\ln\frac{\Delta_g}{|\delta\omega|}, \qquad (15)$$

where $\delta\omega = \omega - \Delta - \Delta_g$ and

$$c_1 = 1 - \frac{\gamma^2 \Delta_g^4}{\Delta^2 \epsilon_g (\epsilon_g - \Delta_g)}. \qquad (16)$$

These expressions imply modifications in the so-called Riedel singularity[35] as compared to the case of usual Josephson junctions between two superconductors. This difference is by no means surprising since the density of states in our metallic dot differs from that of a BCS superconductor. We also observe that the functions $\mathrm{Im}\,\delta S_{1,2}(\omega)$ experience a jump at $\delta\omega = 0$. The magnitude of this jump reads

$$\mathrm{Im}\,\delta S_{1,2} = \frac{\Delta}{2eR_N}\left[\pi\sqrt{\frac{\Delta_g}{\Delta}}\left(\frac{1}{\sqrt{c_1}} - 1\right)\right]. \qquad (17)$$

Finally, we note the presence of peculiarities in the behavior of the functions $\mathrm{Re}\,\delta S_{1,2}(\omega)$ and $\mathrm{Im}\,\delta S_{1,2}(\omega)$ at $\omega = 2\Delta$ (cf. Fig. 2).

IV. NUMERICAL ANALYSIS

Our numerical procedure follows closely that of Ref. 19. We will make use of the representation

$$e^{i\varphi(t)} = e^{ieVt}\sum_{n=-N}^{N} W_n e^{-in\omega_J t}, \qquad (18)$$

where V is the average voltage across the tunnel barrier, $\omega_J = 2eV$ is the Josephson frequency, and W_n are $2N+1$ complex numbers to be determined. As usually, Eq. (18) demonstrates that the higher harmonics of the Josephson frequency are excited in our device.
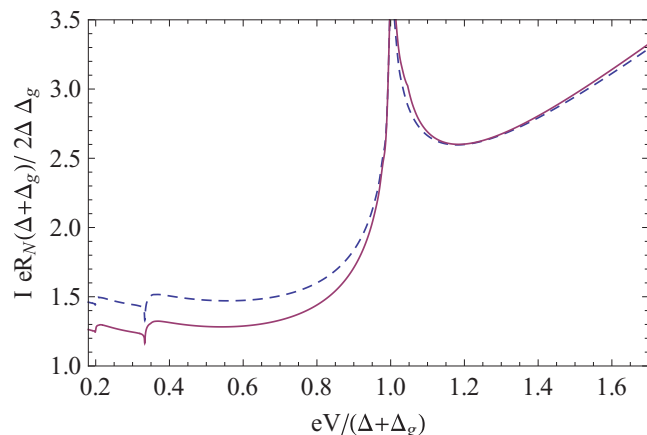

FIG. 3. (Color online) The current through our device as a function of the average voltage at $T \to 0$ for $\epsilon_g/\Delta = 0.95$ and $\gamma = 0.1$ (solid curve). The dashed curve corresponds to the same quantity evaluated with the kernels $\tilde{S}_{1,2}(\Delta, \Delta_g, \omega)$.

Our numerics shows that sufficient accuracy is achieved if one restricts the summation in Eq. (18) by $N = 25$. The numbers W_n are determined bearing in mind that (a) in the current-biased regime considered here only the $n = 0$ component of the current differs from zero, (b) the condition $e^{i\varphi(t)}e^{-i\varphi(t)} = 1$ imposes extra restrictions on W_n, and (c) here we choose $\varphi(t = 0) = 0$, which is equivalent to $\sum_{n=-N}^{N} \mathrm{Im}\,W_n = 0$.

This set of conditions provides $4N + 2$ real equations sufficient to fully determine W_n. Resolving these equations by the Newton's method we finally recover the current through our system as a function of the average voltage V. The results of numerical analysis are displayed in Figs. 3–5.

Similarly to ordinary Josephson junctions between two BCS superconductors[19,20] the I-V curves demonstrate peculiarities at voltage values

$$eV = \frac{\Delta + \Delta_g}{2m + 1}, \qquad (19)$$

where m is an integer number. These peculiarities stem from the Riedel-like singularity contained in the kernels $S_{1,2}$. In
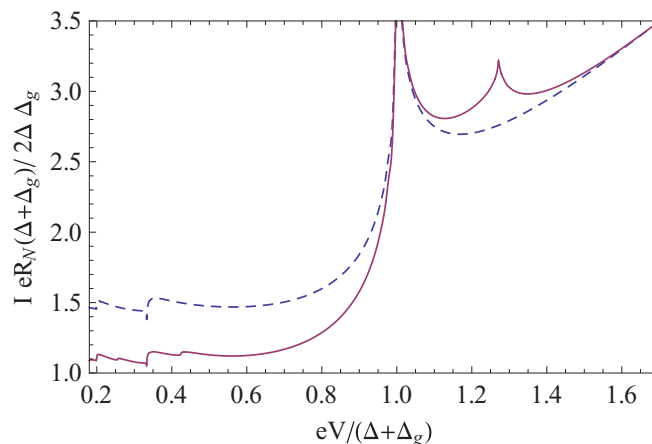

FIG. 4. (Color online) The same as in Fig. 3 for $\epsilon_g/\Delta = 0.95$ and $\gamma = 0.8$.
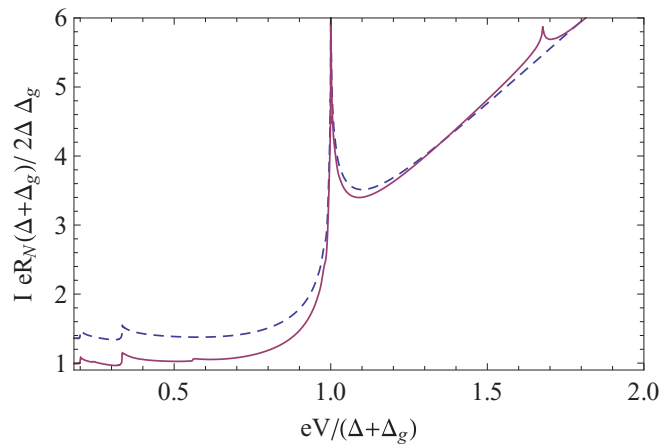
FIG. 5. (Color online) The same as in Fig. 3 for $\epsilon_g/\Delta = 0.95$ and $\gamma = 4$.

addition, we also observe extra peculiarities which occur at voltages

$$eV = \frac{2\Delta}{2m+1}. \tag{20}$$

These latter features are not present in ordinary Josephson junctions at all. In our case these peculiarities are caused by the behavior of kernels $S_{1,2}(\omega)$ at $\omega = 2\Delta$ (see Fig. 2). These additional features on the I-V curve are more pronounced for intermediate values of the electron-hole dephasing parameter $\gamma \sim 1$ and become considerably less pronounced both at small and large values of γ (cf. Fig. 4 with Figs. 3 and 5).

The dependencies presented in Figs. 3–5 demonstrate that at certain values of the bias current the average voltage V becomes multivalued, i.e., there exists more than one different voltage state corresponding to the same bias I. Accordingly, in this regime one can expect to observe jumps between different voltage branches as well as a hysteretic behavior of our device. On the other hand, there also exists a subgap voltage regime where V remains single valued for a fixed bias current. For example, for the parameters employed in Figs. 3–5 such a nonhysteretic regime is realized within the voltage interval

$$0.8 \lesssim \frac{eV}{\Delta + \Delta_g} \lesssim 0.95, \tag{21}$$

which can be conveniently used, e.g., to perform magnetoresistance experiments. An example of the voltage-phase dependence obtained in this region is presented in Fig. 6. These plots demonstrate *negative magnetoresistance*, i.e., the system resistance decreases with increasing magnetic flux Φ. The amplitude of this voltage modulation effect decreases with increasing dephasing parameter γ. Also, for the values of χ sufficiently close to π the hysteretic behavior can be reinstated. For example, for the plots displayed in Fig. 6 this is the case at $\chi \gtrsim 2.5$ (only the subgap branch is shown in this figure; for χ close to π, when Δ_g becomes close to zero for the symmetric case presented in Fig. 6, there can be three solutions for V at given $I \sim \Delta/eR_N$).

Note that the effect of voltage modulation by the external flux persists also at higher voltages $eV > \Delta + \Delta_g$, in which case deviations from the normal state behavior become smaller.
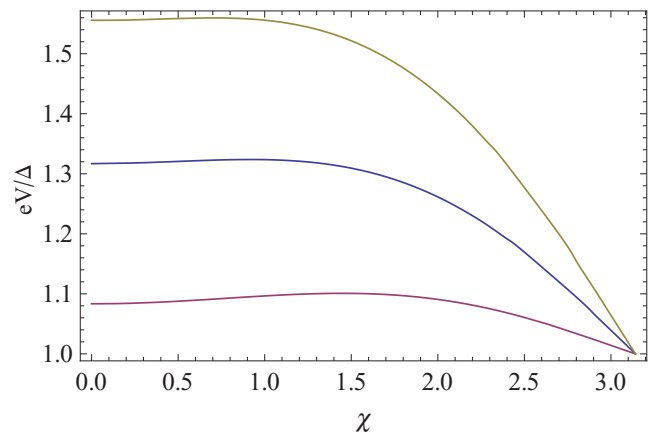

FIG. 6. (Color online) Voltage modulation in a current-biased Andreev interferometer in the low temperature limit. Here we set $G_2 = G_3$ and the parameter γ equal to 0.1, 0.8, and 4 (top to bottom). The corresponding current bias values are 1.4, 1, and 0.5 $\Delta/(eR_N)$.

In this regime the system magnetoresistance turns out to be positive, though the amplitude of the voltage modulations is diminished and becomes vanishingly small for sufficiently large values of γ. This behavior is exemplified in Fig. 7.

V. DISCUSSION

In this work we analyzed the behavior of an Andreev interferometer in the current-biased regime. As compared to the voltage-biased regime studied before,[7] we discover a rather different form of the I-V curves and observe some peculiarities, e.g., at voltage values defined in Eqs. (19) and (20). Singularities at voltages (19) are due to the Riedel-like feature and are qualitatively similar to those observed in experiments with ordinary Josephson junctions.[21] Additional features at voltages (20) are specific to systems under consideration and are not present, e.g., in tunnel junctions between two BCS superconductors.

An experimental observation of the above two series of singularities in Andreev interferometers under consideration would be highly interesting as, for instance, it would allow to
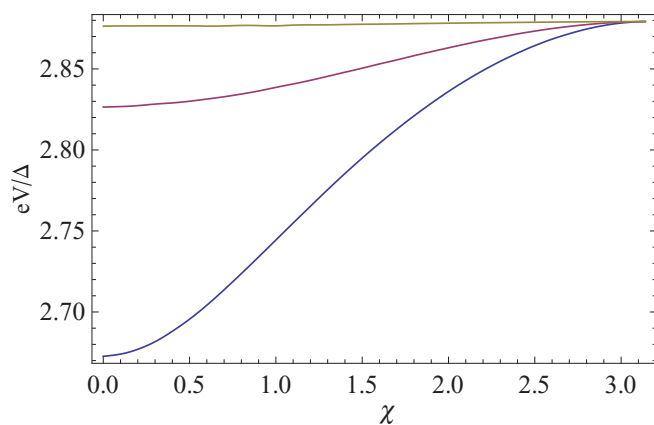

FIG. 7. (Color online) The same as in Fig. 6 at higher bias current value $I = 2.7\Delta/(eR_N)$. The values of γ are 0.1, 0.8, and 4 (bottom to top).

accurately determine the parameters of such devices. Indeed, the dephasing parameter γ can be determined with the aid of Eq. (10), e.g., by setting an external magnetic flux equal to zero $\Phi = 0$ (and, hence, $\epsilon_g = \Delta$). Having established this parameter, one can also verify the flux dependence $\epsilon_g(\Phi)$ (11) at all values of Φ and also obtain extra information about the conductances G_2 and G_3.

Depending on the value of the applied external current, Andreev interferometers can show either hysteretic or non-hysteretic behavior. The latter behavior is well suited to study the effect of voltage modulation by an external magnetic flux. For example, within the voltage interval (21), one observes negative magnetoresistance and a significant voltage modulation effect (cf. Fig. 6) which is sufficient for the reliable performance of Andreev interferometers.

Let us also note that the above features of Andreev interferometers predicted here, such as hysteretic behavior, peaks in the differential resistance, and negative magnetoresistance, have been observed in recent experiments.[36] It appears, however, that more work will be needed in order to perform a quantitative comparison between theory and experiment.

To complete our discussion we briefly address the effect of voltage noise. Denoting the voltage fluctuation by $\delta V(t)$, introducing the voltage-voltage correlation function

$$S_V(\omega) = \int d(t_1 - t_2) e^{i\omega(t_1 - t_2)} \langle \delta V(t_1) \delta V(t_2) \rangle , \quad (22)$$

and following the analysis developed in Ref. 37 for the case of ordinary Josephson junctions (see also Ref. 20), in the limit of low frequencies for $eV \lesssim 2\Delta$ we arrive at an estimate

$$S_V(0) \sim \Delta R_d^2 / R_N, \quad R_d = dV/dI. \quad (23)$$

We note that within voltage interval (21) the differential resistance of our device obeys the inequality $R_d \lesssim R_N$ (see Figs. 3–5). Since the voltage modulation for small γ is $\sim \Delta/e$ (see Fig. 6), a typical noise-to-signal ratio (ζ) of our device can be estimated as

$$\zeta \lesssim \sqrt{(R_N/R_q)(\delta\omega/\Delta)}. \quad (24)$$

Here R_q is the quantum resistance unit and $\delta\omega$ defines the bandwidth for our system. As here we are interested in the averaged voltage and as higher Josephson harmonics should be effectively filtered out, we may set $\delta\omega \ll \Delta$. In addition, we will assume that $R_N \ll R_q$. In this case the estimate (24) yields $\zeta \ll 1$. Perhaps we may also add that, as it was concluded in recent experiments,[5,36] the intrinsic noise of Andreev interferometers was lower than that in employed readout electronics. This observation, combined with the estimate (24), appears to indicate that voltage noise may remain sufficiently weak and will not compromise the performance of Andreev interferometers.

APPENDIX

In the case of a tunnel barrier between two BCS superconductors the expressions for $S_{1,2}$ (6) reduce to the well-known results[32,33] which can be briefly summarized as follows. Following Werthamer,[32] let us introduce the notations

$$x = \frac{|\omega|}{\Delta_1 + \Delta_2}, \quad \delta = \frac{|\Delta_1 - \Delta_2|}{\Delta_1 + \Delta_2}. \quad (A1)$$

Then at $T \to 0$ we find

$$\tilde{S}_1(\omega) = \frac{2\Delta_1\Delta_2}{eR_N(\Delta_1 + \Delta_2)} \left[\frac{1}{\sqrt{1-x^2}} K\left(\frac{\delta^2 - x^2}{1 - x^2}\right) - \frac{2\sqrt{1-x^2}}{1 - \delta^2} E\left(\frac{\delta^2 - x^2}{1 - x^2}\right) \right], \quad 0 \leqslant x \leqslant \delta,$$

$$\tilde{S}_1(\omega) = \frac{2\Delta_1\Delta_2}{eR_N(\Delta_1 + \Delta_2)} \frac{1}{\sqrt{1-\delta^2}} \left[K\left(\frac{x^2 - \delta^2}{1 - \delta^2}\right) - 2E\left(\frac{x^2 - \delta^2}{1 - \delta^2}\right) \right], \quad \delta \leqslant x \leqslant 1, \quad (A2)$$

$$\tilde{S}_1(\omega) = \frac{2\Delta_1\Delta_2}{eR_N(\Delta_1 + \Delta_2)} \left\{ \frac{2\sqrt{x^2 - \delta^2}}{1 - \delta^2} \left[K\left(\frac{1 - \delta^2}{x^2 - \delta^2}\right) - E\left(\frac{1 - \delta^2}{x^2 - \delta^2}\right) \right] - \frac{1}{\sqrt{x^2 - \delta^2}} K\left(\frac{1 - \delta^2}{x^2 - \delta^2}\right) \right.$$

$$\left. + i\,\mathrm{sgn}\,\omega \left[\frac{2\sqrt{x^2 - \delta^2}}{1 - \delta^2} E\left(\frac{x^2 - 1}{x^2 - \delta^2}\right) - \frac{1}{\sqrt{x^2 - \delta^2}} K\left(\frac{x^2 - 1}{x^2 - \delta^2}\right) \right] \right\}, \quad x \geqslant 1,$$

and

$$\tilde{S}_2(\omega) = \frac{2\Delta_1\Delta_2}{eR_N(\Delta_1 + \Delta_2)} \frac{1}{\sqrt{1-x^2}} K\left(\frac{\delta^2 - x^2}{1 - x^2}\right), \quad 0 \leqslant x \leqslant \delta,$$

$$\tilde{S}_2(\omega) = \frac{2\Delta_1\Delta_2}{eR_N(\Delta_1 + \Delta_2)} \frac{1}{\sqrt{1-\delta^2}} K\left(\frac{x^2 - \delta^2}{1 - \delta^2}\right), \quad \delta \leqslant x \leqslant 1, \quad (A3)$$

$$\tilde{S}_2(\omega) = \frac{2\Delta_1\Delta_2}{eR_N(\Delta_1 + \Delta_2)} \frac{1}{\sqrt{x^2 - \delta^2}} \left[K\left(\frac{1 - \delta^2}{x^2 - \delta^2}\right) + i\,\mathrm{sgn}\,\omega K\left(\frac{x^2 - 1}{x^2 - \delta^2}\right) \right], \quad x \geqslant 1,$$

where

$$K(k) = \int_0^{\pi/2} \frac{d\phi}{\sqrt{1 - k\sin^2\phi}}, \quad E(k) = \int_0^{\pi/2} d\phi\sqrt{1 - k\sin^2\phi} \tag{A4}$$

are complete elliptic integrals. At $x \to 1$ these expressions diverge demonstrating the so-called Riedel singularity[35]

$$\operatorname{Re}\tilde{S}_1(\omega) \approx \frac{\sqrt{\Delta_1\Delta_2}}{2eR_N}\left[\ln\left(\frac{8(1-\delta^2)}{|1-x|}\right) - 4\right], \quad \operatorname{Re}\tilde{S}_2(\omega) \approx \frac{\sqrt{\Delta_1\Delta_2}}{2eR_N}\ln\left(\frac{8(1-\delta^2)}{|1-x|}\right). \tag{A5}$$

[1] V. T. Petrashov, V. N. Antonov, P. Delsing, and R. Claeson, Phys. Rev. Lett. **70**, 347 (1993); JETP Lett. **60**, 589 (1994); Phys. Rev. Lett. **74**, 5268 (1995).

[2] P. G. N. de Vegvar, T. A. Fulton, W. H. Mallison, and R. E. Miller, Phys. Rev. Lett. **73**, 1416 (1994); H. Pothier, S. Guéron, D. Esteve, and M. H. Devoret, *ibid.* **73**, 2488 (1994).

[3] V. T. Petrashov, K. G. Chua, K. M. Marshall, R. Sh. Shaikhaidarov, and J. T. Nicholls, Phys. Rev. Lett. **95**, 147001 (2005).

[4] I. Sosnin, H. Cho, V. T. Petrashov, and A. F. Volkov, Phys. Rev. Lett. **96**, 157002 (2006).

[5] M. Meschke, J. T. Peltonen, J. P. Pekola, and F. Giazotto, Phys. Rev. B **84**, 214514 (2011).

[6] F. Giazotto and F. Taddei, Phys. Rev. B **84**, 214502 (2011).

[7] A. V. Galaktionov, A. D. Zaikin, and L. S. Kuzmin, Phys. Rev. B **85**, 224523 (2012).

[8] J. Lantz, V. S. Shumeiko, E. Bratus, and G. Wendin, Phys. Rev. B **65**, 134523 (2002).

[9] E. V. Bezuglyi, V. S. Shumeiko, and G. Wendin, Phys. Rev. B **68**, 134506 (2003).

[10] K. K. Likharev, Rev. Mod. Phys. **51**, 101 (1979).

[11] R. de Bruyn Ouboter and A. N. Omelyanchouk, Superlatt. Microstruct. **25**, 1005 (1999).

[12] A. N. Omelyanchouk and M. Zareyan, Physica B **291**, 81 (2000).

[13] J. C. Cuevas and H. Pothier, Phys. Rev. B **75**, 174513 (2007).

[14] B. Reulet, J. Senzier, and D. E. Prober, Phys. Rev. Lett. **91**, 196601 (2003).

[15] L. S. Levitov and M. Reznikov, Phys. Rev. B **70**, 115305 (2004).

[16] A. V. Galaktionov, D. S. Golubev, and A. D. Zaikin, Phys. Rev. B **68**, 235333 (2003).

[17] J. Salo, F. W. J. Hekking, and J. P. Pekola, Phys. Rev. B **74**, 125427 (2006).

[18] M. Kindermann, Yu. V. Nazarov, and C. W. J. Beenakker, Phys. Rev. B **69**, 035336 (2004).

[19] D. G. McDonald, E. G. Johnson, and R. E. Harris, Phys. Rev. B **13**, 1028 (1976).

[20] K. K. Likharev, *Dynamics of Josephson Junctions and Circuits* (Gordon and Breach, Amsterdam, 1986).

[21] J. Niemeyer and V. Kose, Appl. Phys. Lett. **29**, 380 (1976).

[22] R. E. Howard, E. L. Hu, L. D. Jackel, L. A. Fetter, and R. H. Bosworth, Appl. Phys. Lett. **35**, 879 (1979); L. D. Jackel, E. L. Hu, R. E. Howard, L. A. Fetter, and D. Tennant, IEEE Trans. Magn. **17**, 295 (1981).

[23] G. Dousselin and J. Rosenblatt, J. Appl. Phys. **51**, 802 (1980).

[24] R. F. Broom, A. Oosenbrug, and W. Walter, Appl. Phys. Lett. **37**, 237 (1980).

[25] P. A. Bobbert, R. Fazio, G. Schön, and A. D. Zaikin, Phys. Rev. B **45**, 2294 (1992).

[26] A. A. Golubov, F. K. Wilhelm, and A. D. Zaikin, Phys. Rev. B **55**, 1123 (1997).

[27] Yu. V. Nazarov and T. H. Stoof, Phys. Rev. Lett. **76**, 823 (1996).

[28] G. Schön and A. D. Zaikin, Phys. Rep. **198**, 237 (1990).

[29] A. D. Zaikin, Physica B **203**, 255 (1994).

[30] I. Snyman and Yu. V. Nazarov, Phys. Rev. B **77**, 165118 (2008).

[31] A. V. Galaktionov and A. D. Zaikin, Phys. Rev. B **82**, 184520 (2010).

[32] N. R. Werthamer, Phys. Rev. **147**, 255 (1966).

[33] A. I. Larkin and Yu. N. Ovchinnikov, Sov. Phys. JETP **24**, 1035 (1967).

[34] Our C++ numerical code is available upon request.

[35] E. Riedel, Z. Naturforsch. A **19**, 1634 (1964).

[36] J. Wells, C. Shelly, and V. T. Petrashov (unpublished).

[37] A. B. Zorin, Sov. J. Low Temp. Phys. **7**, 709 (1981).